

Measurement of weak bosons Single Spin Asymmetry in Transversely Polarized p-p Collisions at RHIC

Salvatore Fazio*and Dmitri Smirnov[†]

Physics Department, Brookhaven National Lab

June 28, 2015
v4.0

Abstract

The present study is the first attempt to measure the single spin asymmetry for weak bosons produced in transversely polarized proton collisions at STAR by a complete reconstruction of the boson kinematics. The measured observable is sensitive to the non universality of the Sivers function, which has its origin in the rescattering of the struck parton in the color field of the remnant of the polarized proton. Furthermore, W production provides an ideal tool to study the spin-flavor structure of the proton, specifically the light sea-quarks at the scale of the W mass and therefore tests the evolution of the transverse momentum dependent parton distribution functions.

*sfazio@bnl.gov

[†]dsmirnov@bnl.gov

Contents

1	Introduction	3
2	Preliminary Sensitivity Studies	3
3	The W^\pm selection and reconstruction	5
3.1	Transverse momentum reconstruction	6
3.1.1	Dependence of the MC correction by the charge sign	8
3.1.2	Dependence of the MC correction by the ZDC rates	8
3.1.3	Dependence of the MC correction by the PYTHIA tuning	8
3.2	Longitudinal momentum reconstruction	9
3.3	Resolution	11
3.4	Background estimation	13
3.5	Systematic uncertainties	17
4	Average polarization	17
5	Asymmetry measurement	18
6	The Z^0 selection and asymmetry measurement	20
7	Conclusions and Outlook	23
A	Extraction of the analyzing power, A_N	25
B	Reproduction of results	25
B.1	How to check out and build the analysis code	25
B.2	How to split the Monte Carlo file lists	26
B.3	How to produce the analysis ROOT trees	27
B.4	How to check condor jobs output	27
B.5	How to produce histograms from ROOT trees	27
C	Run list	27

1 Introduction

The present study is the first attempt to measure the single spin asymmetry for weak bosons produced in transversely polarized proton collisions at STAR by a complete reconstruction of the boson kinematics.

Transversely polarized spin effects have been an extremely active topic among experiment and theory in the past years, because of their connection to transverse momentum dependent (TMD) distributions (leading to a multi-dimensional picture of the proton) and a possible test of the framework and the underlying theory of perturbative QCD. For a quantitative application of the TMD framework to transverse single-spin asymmetries measured in proton-proton collisions, the required two scales (typically Q^2 and p_T) are not well defined, excepted for Drell-Yan di-lepton (DY) and W^\pm/Z^0 boson production. DY has been at the center of attention for the non-universality test of the so-called Sivers TMD function, f_{1T}^\perp , which describes the correlation of parton transverse momentum with the transverse spin of the nucleon. There is evidence of a quark Sivers effect in Semi-Inclusive Deep Inelastic Scattering (SIDIS) measurements where the quark Sivers function is associated with a final state effect from the gluon exchange between the struck quark and the target nucleon remnants. On the other hand, for the virtual photon production in the Drell-Yan process, the Sivers asymmetry appears in the initial state of the interaction. As a consequence, the quark Sivers functions are of opposite sign in SIDIS and in Drell-Yan

$$f_{q/h^\uparrow}^{\text{SIDIS}}(x, k_\perp) = -f_{q/h^\uparrow}^{\text{DY}}(x, k_\perp). \quad (1)$$

The experimental test of this sign change is one of the open questions in hadronic physics, and can provide insights on the TMD factorization. While luminosities required for a meaningful measurement of asymmetries in Drell-Yan production are challenging, W^\pm and Z^0 bosons production is equally sensitive to the predicted sign change and can be well measured at the STAR experiment. The results can also provide essential input to study the new theoretical concept of evolution effects of transverse momentum dependent distribution functions, because of the high Q^2 in the W^\pm/Z^0 production due to the large boson mass. The STAR experiment at RHIC is currently the only place in the world where these effects can be tested.

The transverse single spin asymmetry, A_N , has been derived in [1] and its parametrization is based on the fits to SIDIS data. Predictions show that a transverse asymmetry solely calculated from the lepton decay is diluted [1] if compared to the same asymmetry calculated directly from the produced boson. Thus, a full reconstruction of the produced boson kinematics is crucial for a meaningful measurement. The present analysis is based on a data sample collected in the year 2011 at STAR using transversely polarized proton-proton collisions at the center-of-mass energy of $\sqrt{s} = 500$ GeV, the total integrated luminosity is $L_{\text{int}} = 25 \text{ pb}^{-1}$. In the present work we use this exploratory run to test the possibility of fully reconstructing the W^\pm boson kinematics at STAR, using the lepton decay and all other particles in the recoil from the initial hard scattering. This analysis also includes a first look at A_N in Z^0 production.

2 Preliminary Sensitivity Studies

In 2011 transversely polarized proton-proton beams were brought into collisions at STAR with a center of mass energy of 500 GeV. In this regime the W is expected to have a relatively small P_T . We use PYTHIA 6.8 to simulate $W^\pm \rightarrow e^\pm \nu_e$ to the LO with unpolarized beams. Expected kinematic distributions of the lepton coming from the W decay is shown in Figure 1.

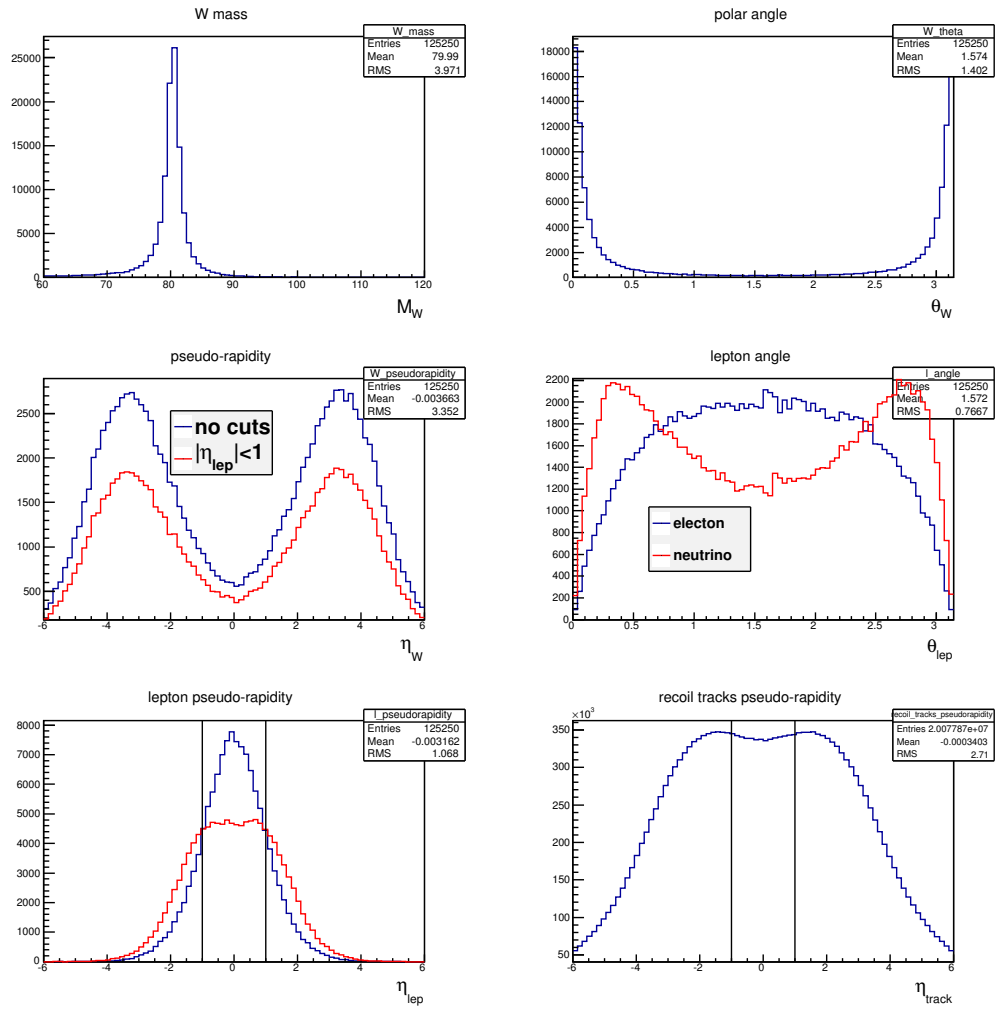


Figure 1: W-mass; polar angles and pseudo rapidity distributions of the produced W, the decay leptons and the recoil tracks.

Our aim is to use Monte Carlo to correct for the missing P_T in the recoil tracks due to the limited acceptance of the STAR detector.

3 The W^\pm selection and reconstruction

In this analysis, data were recorded using a calorimeter trigger requirement of 12 GeV of transverse energy E_T in a $\Delta\eta \times \Delta\phi$ region of $\sim 0.1 \times 0.1$ of the BEMC. namely the 2011 TriggerID 320801.

A data sample characterized by the $W \rightarrow e\nu$ signature has been selected, mostly requiring an isolated high P_T electron. We adopt the same selection procedure already used (and described in details) at STAR for weak boson production measurements of polarized longitudinal single-spin asymmetry [2–5] and unpolarized cross section [9, 10].

We define a P_T -balance variable, \vec{P}_T^{bal} , as the vector sum of the decay electron \vec{P}_T^e and the transverse momentum of the hadronic recoil.

$$\vec{P}_T^{bal} = \vec{P}_T^e + \vec{P}_T^{recoil} = \vec{P}_T^e + \sum_{i \in \text{tracks, clusters}} \vec{P}_{i,T},$$

Differently from previous STAR weak boson analyses where a jet reconstruction cone algorithm has been used, in the present work \vec{P}_T^{recoil} is calculated as the vectorial sum of the transverse momentum of all the tracks not belonging to the decay electron candidate and all the trackless clusters in the BEMC with an energy above the noise threshold of 200 MeV.

The scalar variable signed- P_T -balance, defined as $\text{signed-}P_T^{bal} = (\vec{P}_T^{bal} \cdot \vec{P}_T^e) / |\vec{P}_T^e|$, is used to suppress the QCD background, for details see [2–5].

The selection criteria are the following

- One isolated electron
 - lepton- $P_T > 25$ GeV;
 - $\text{Track-}|\eta| < 1$;
 - Isolation criterium: $(P^{track} + E^{cluster}) / \Sigma[P^{tracks} \text{ in } R=0.7 \text{ cone}] > 0.9$;
 - track coming from the maximum ranked vertex;
- $|Z_{vertex}| < 100$ cm; vertex rank > 0 ;
- signed- $P_T^{bal} > 18$ GeV, suppresses QCD back ground;
- $0.4 < |\text{Charge(TPC)} * E_T(\text{EMC}) / P_T(\text{TPC})| < 1.8$, minimizes charge misidentification.

In the present analysis we also ask $P_T^{recoil} > 0.5$ GeV to minimize the systematics uncertainties in reconstructing the W boson transverse momentum as described in Sec. 3.1.

At the end we can identify two data samples depending on the electron charge; a positive charge identifies our W^+ signal whereas a negative charge marks our W^- signal. After the whole selection procedure, the following events survive

- positive-charged electron (W^+ signal): 1216 events;
- negative-charged electron (W^- signal): 332 events.

3.1 Transverse momentum reconstruction

In order to fully reconstruct the W kinematics, the momenta of all W -decay products must be measured. The momentum of the neutrino produced in the leptonically decayed W cannot be measured and can only be indirectly deduced from momentum conservation. In the W events produced at $\sqrt{s} = 500$ GeV at STAR we can assume that most of the missing transverse momentum is carried by the neutrino from the W decay. This assumption is based on the fact that only very little energy is left for anything other than W production from the primary hard scattering. In the transverse plane the initial momentum of the system of interacting partons is negligible and so must be the vector sum of all final particles momenta. We calculate the transverse momentum of the produced W as

$$\vec{P}_T^W = -\vec{P}_T^{recoil} = - \sum_{\substack{i \in \text{tracks,} \\ \text{clusters}}} \vec{P}_{i,T}. \quad (2)$$

In a typical collider detector like STAR the problem with measuring the missing momentum from the hadronic recoil is that particles with very high rapidities escape the detector. At the same time, the beam remnants with high longitudinal momentum carry away only a little portion of the total transverse momentum. We accounted for the non measured tracks and clusters by using the following event-by-event Monte Carlo correction to the data

$$k_i = \frac{P_{T,i}^W(true)}{P_{T,i}^{recoil}(reconstructed)}, \quad (3)$$

where $P_{T,i}^W(true)$ is the generated P_T of the W at MC level and $P_{T,i}^{recoil}(reconstructed)$ is the P_T of the recoil reconstructed after a full GEANT simulation of the detector in each i -th bin. The distribution of the correction factor, k , versus the recoil P_T is shown in Fig. 2. The correction has been applied to the data on an event-by-event base as follows

1. read the i -th bin of recoil- P_T from data;
2. do a Y-Projection the correction factor from Fig. 2 in the corresponding i -th bin;
3. normalize the projection distribution to 1;
4. use a random generator to select a correction value from the normalized projection distribution.

A MC test shows that after the correction has been applied, data are in a very good agreement with predictions from RhicBOS and PYTHIA, as shown in Fig. 3. In reconstructing the hadronic recoil from the tracks and clusters, additional cuts have been applied to avoid the very low total recoil- P_T , when most of the tracks fall off the STAR tracker (TPC) acceptance

- Total $P_T^{recoil} > 0.5$ GeV;
- P_T of each single track in the recoil > 0.2 GeV.

Figure 4 shows how the data/MC agreements improves requiring a minimum recoil- P_T value of 0.5 GeV compared with a lower or no threshold. The final data/MC agreement for reconstructing the W boson transverse momentum over an extended range is shown in Fig. 9(left).

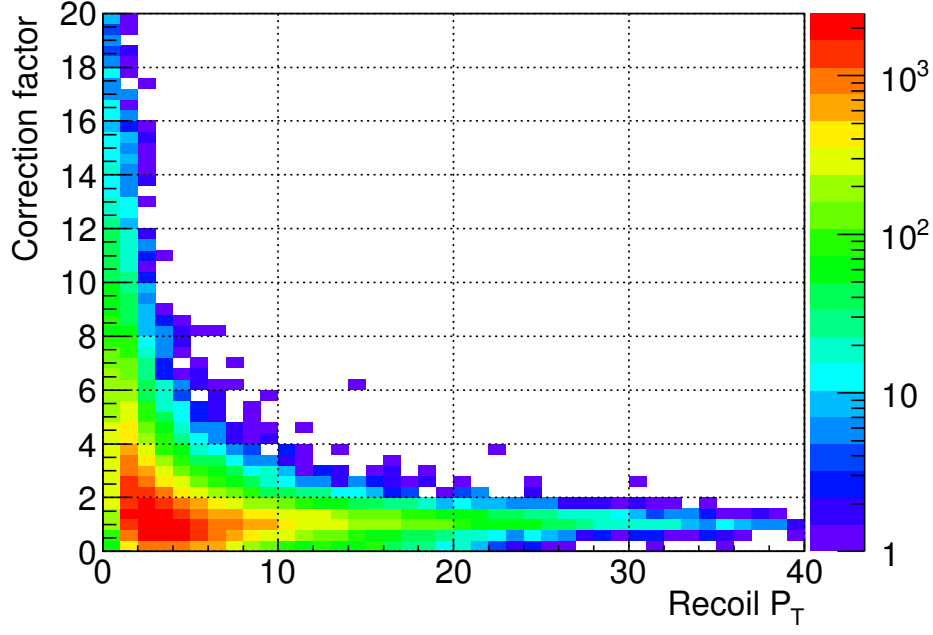


Figure 2: Distribution of the correction factor, k , versus the recoil P_T .

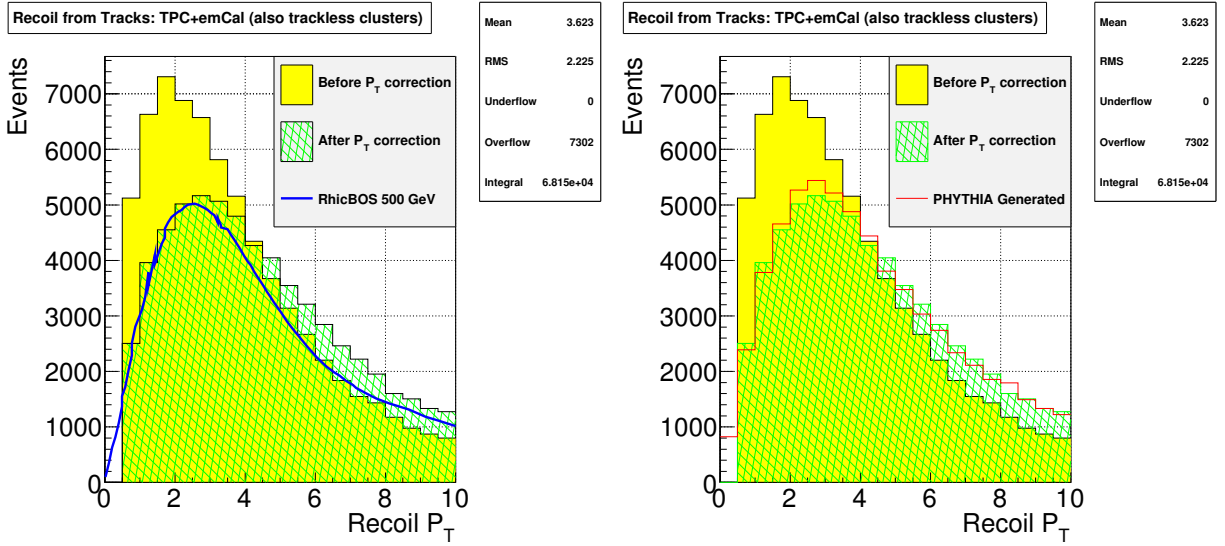


Figure 3: Data before and after the P_T correction has been applied are compared with predictions from RhicBOS (*left*) and PYTHIA (*right*).

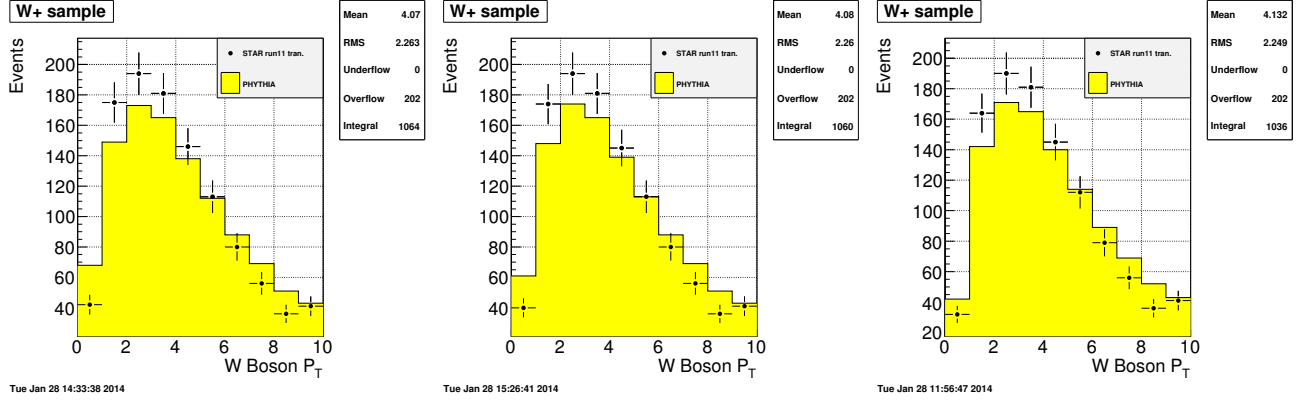


Figure 4: Data/MC agreement for the total recoil- P_T with a minimum value of $P_T > 0.2$ GeV (left), $P_T > 0.3$ GeV (center) and $P_T > 0.5$ GeV (right).

3.1.1 Dependence of the MC correction by the charge sign

Though not expected, a possible dependence of the correction factor by the boson charge has been tested by independently using an embedded W^- Monte Carlo sample for its calculation. Fig. 5 (top left) shows a comparison of the projected correction factor in each Recoil P_T bin, calculated using W+ and W- samples independently. This comparison shows that the boson charge has no effect on the correction factor.

3.1.2 Dependence of the MC correction by the ZDC rates

Since the $W - P_T$ reconstruction technique relies on embedded Monte Carlo samples, a possible dependence of the correction factor by the ZDC rates of the zero-bias runs used for embedding has been investigated. The ZDC rate of 2011 pp zero-bias events ranges between 40k and 95k. In order to test a dependence on the ZDC rate, a subsample of zero-bias runs with a rate < 90 k, corresponding to a total of 7 runs, has been selected and the corresponding embedded MC sample used to reconstruct $W - P_T$. Fig. 5 (top right) shows a comparison of the projected correction factor in each Recoil P_T bin using only the subsample of zero-bias events with high ZDC rates and using the whole sample of zero bias events. The high rate sample contains much less statistics, thus suffering higher fluctuation. From the comparison we can easily conclude that in run 2011 there is no sizable difference in calculating the correction factor due to ZDC rates of zero-bias embedding runs.

3.1.3 Dependence of the MC correction by the PYTHIA tuning

The Monte Carlo sample used for the correction factor calculation has been simulated with PYTHIA 6.4 using the “Perugia tune” and setting $\text{PARP}(91) = 2$ and $\text{CKIN}(3) = 10$. The choice of the Perugia tuning follows the study shown in Fig. 6, where samples generated with different tunings are compared with an independent prediction from RhicBOS Monte Carlo [6], from Altarelli et al. [7] and the UA1 experimental data [8]. It is evident that “tune A” generates a peak that is shifted to lower boson P_T values. Thus, it is to be expected that the correction factor will show a dependence on the tuning used for the simulation. To test this dependence, we used a Monte Carlo sample simulated using PYTHIA Tune A, $\text{PARP}(91)=1$, $\text{CKIN}(3)=1$ in calculating the correction factor and compare this with our original tuning, as shown in Fig. 5

(bottom). One can see that the correction factor shows a dependence on the PYTHIA tuning for boson $P_T < 10$ GeV. It is also important to stress that, although we put ourselves in the most extreme case comparing very different tunings, the discrepancy of the average correction factor is always much smaller than the standard deviation.

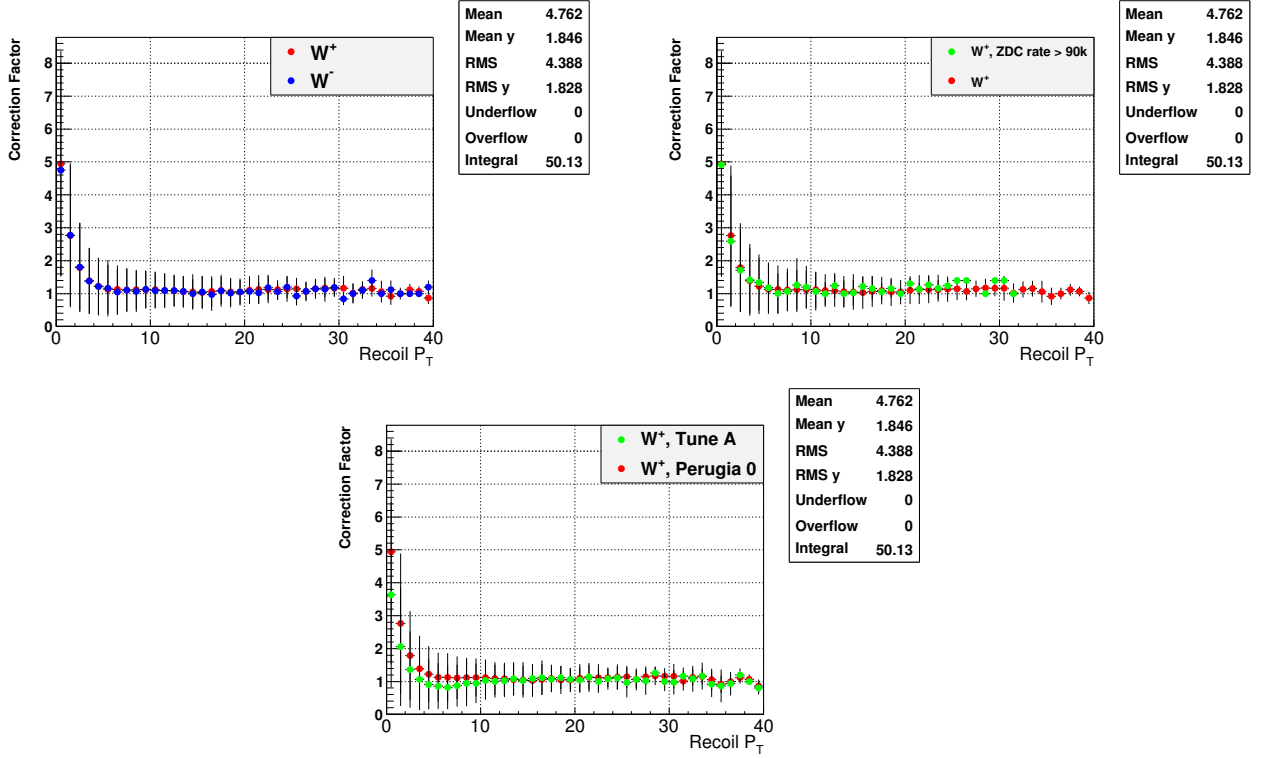


Figure 5: Comparison of the Correction Factor used in the present analysis (*red dots*) with the same factor calculated using a Monte Carlo sample of W^- events (*top left*), a sample only using high ZDC rate zero-bias runs for embedding (*top right*), and a sample using PYTHIA Tune A, PARP(91)=1, CKIN(3)=1 (*bottom*). To facilitate the comparison, the correction factor in each recoil- P_T bin had been projected, the dots correspond to the average value of the distribution in the corresponding bin, whereas the bars correspond to the standard deviation.

3.2 Longitudinal momentum reconstruction

Knowing its transverse momentum, the longitudinal component of the neutrino's momentum can be reconstructed solving the quadratic equation for the invariant mass of the produced boson

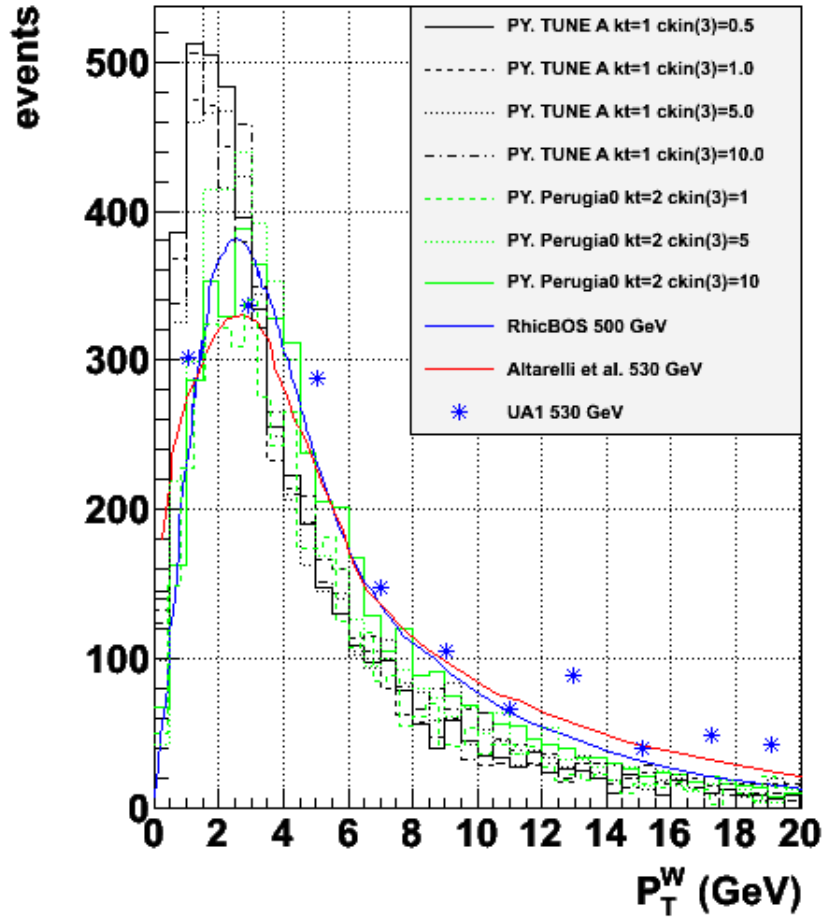
$$M_W^2 = (E_e + E_\nu)^2 - (\vec{P}_e + \vec{P}_\nu)^2, \quad (4)$$

which leads to

$$M_W^2/2 = |\vec{p}_l| |\vec{p}_\nu| - \vec{p}_{l,T} \cdot \vec{p}_{\nu,T} - \vec{p}_{l,z} \cdot \vec{p}_{\nu,z}, \quad (5)$$

where we neglected the masses of the both neutrino and lepton. Introducing a shorthand expression for $A = M_W^2/2 + \vec{p}_{l,T} \cdot \vec{p}_{\nu,T}$, after trivial arithmetics we arrive to a quadratic equation

PYTHIA tuning



Tue Aug 27 16:45:56 2013

Figure 6: The W boson P_T distribution, generated using different PYTHIA tunings, is compared with RhicBOS Monte Carlo [6], with the theoretical prediction from Altarelli et al. [7] and with the UA1 experimental data [8].

$$|\vec{p}_{l,T}|^2 p_{\nu,z}^2 - 2A p_{l,z} p_{\nu,z} + |\vec{p}_{\nu,T}|^2 |\vec{p}_l|^2 - A^2 = 0. \quad (6)$$

In solving this equation we assumed the nominal value of the W -mass. Thus, Eq. 4 leads to two possible solutions for the longitudinal component of the neutrino (and thus the W) momentum

$$p_{\nu,z} = \frac{A p_{l,z} \pm \sqrt{A^2 p_{l,z}^2 - |\vec{p}_{l,T}|^2 (|\vec{p}_{\nu,T}|^2 |\vec{p}_l|^2 - A^2)}}{|\vec{p}_{l,T}|^2}. \quad (7)$$

To distinguish between the two solutions, from now on we name “first solution” the one with the smaller absolute value and “second solution” the remnant one. In order to choose which solution should be used, the fraction of correctly reconstructed events for each solution was estimated via MC. The MC distribution of the reconstructed P_L^W versus the generated level one is shown in Fig. 7 for both solutions separately. To estimate the amount of “well reconstructed” events we considered all the events with a reconstructed longitudinal moments within 30 GeV from the generated value (the two black limit-lines in Fig. 7). The overall fraction of well reconstructed events, estimated according to this criterium, is shown for both solutions separately in the upper side of each plot in Fig. 7. Thus, we investigated the fraction of well reconstructed events in bins of generated P_L^W , as

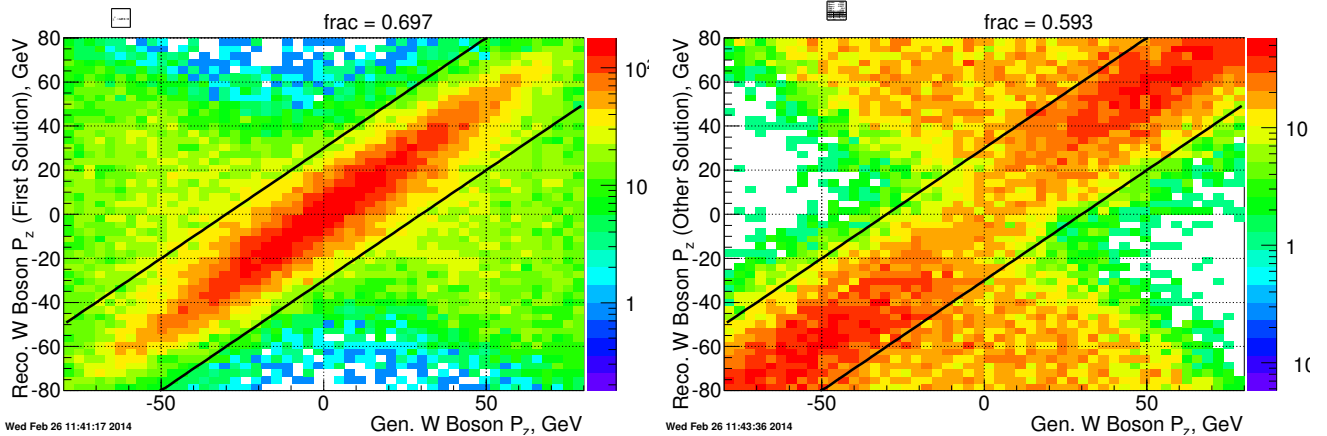


Figure 7: MC distribution of reconstructed versus generated P_L^W for the first solution (*left*) and the second solution (*right*) respectively.

shown in Fig. 8. It is evident that the first solution better reconstructs $P_L^W < 40$ GeV whereas the second solution works better for larger longitudinal momenta. Having in mind that our W bosons are often produced with a longitudinal momentum smaller than 40 GeV, we chose the solution smaller in magnitude, namely the first solution, to reconstruct the boson kinematics because it leads to a much smaller fraction of mis-reconstructed events in our kinematic domain. A data/MC comparison for the P_L^W after all the reconstruction is done, is shown in Fig. 9(*right*). One can see how the momentum of the produced W boson can be fully reconstructed with a satisfactory data/MC agreement.

3.3 Resolution

The expected resolution of the relevant kinematic variables has been studied using PYTHIA 6.4 simulated samples using the “Perugia 0 tune” and setting $k_T = 2$ and $CKIN(3) = 10$. In studying

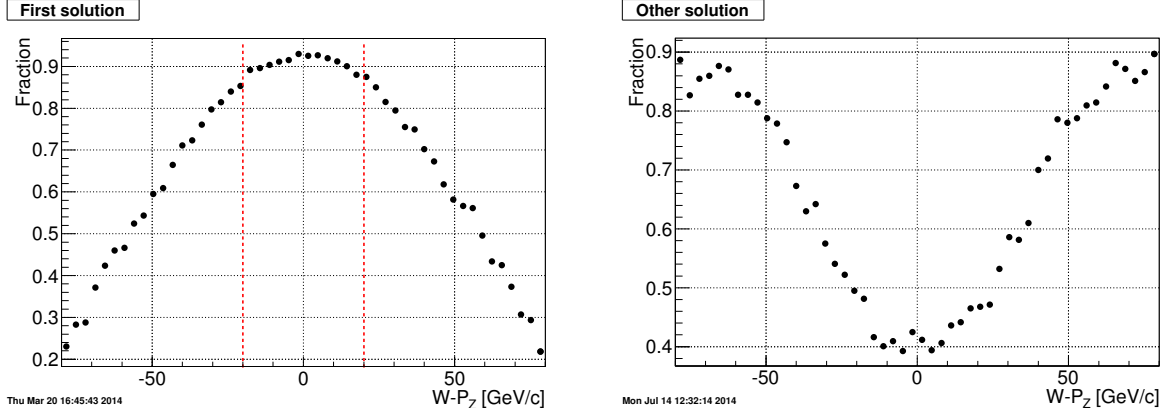


Figure 8: Estimated fraction of well reconstructed events as a function of generated P_L^W for the first solution (*left*) and the second solution (*right*) respectively.

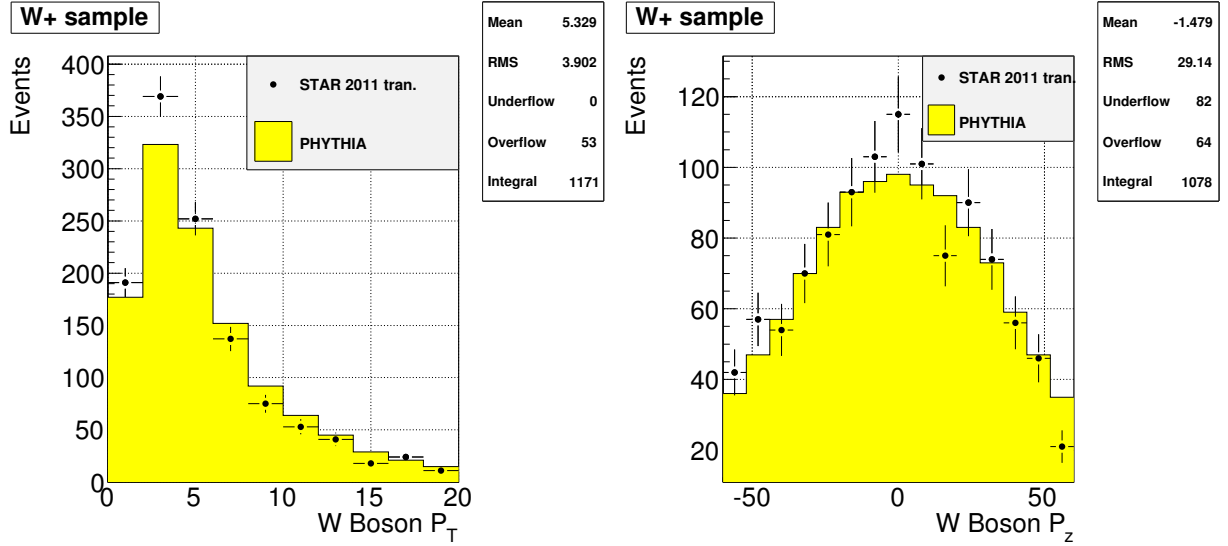


Figure 9: Data/MC agreement for the W boson P_T (*left*) and P_L (*right*).

1 the Recoil- P_T resolution we compared the total sum of recoil- P_T at the generated and reconstructed
2 level in the same boson y and P_T bins used for the final asymmetry measurement, see Sec. 5. An
3 acceptance cut of $|\eta| < 1$ corresponding to the acceptance of the STAR calorimeter has been
4 imposed at the generation level.

5 Due to the random character of the event-by-event P_T correction procedure, the correlation
6 between the generated and reconstructed P_T in a single event is lost. Therefore the evaluation of
7 the resolution has been done without applying the correction procedure. The relative resolution
8 for recoil- P_T has been evaluated looking at the standard deviation of the $\frac{P_T^{Gen} - P_T^{Rec}}{P_T^{Gen}}$ distribution.
9 Fig. fig:reso-pt shows that the relative resolution on recoil- P_T decreases from $\sim 50\%$ in the first
10 bins down to $\sim 30\%$ in the last bin.

11 In the case of the boson rapidity, the relative resolution calculation is sensitive to dividing for
12 $y^{Gen} \sim 0$ and we opted for calculating the absolute resolution as the standard deviation of the
13 $y^{Gen} - y^{Rec}$ distribution. Fig. fig:reso-y shows that the absolute resolution in each of the three
14 y^W -bins is estimated to be ~ 0.1 .

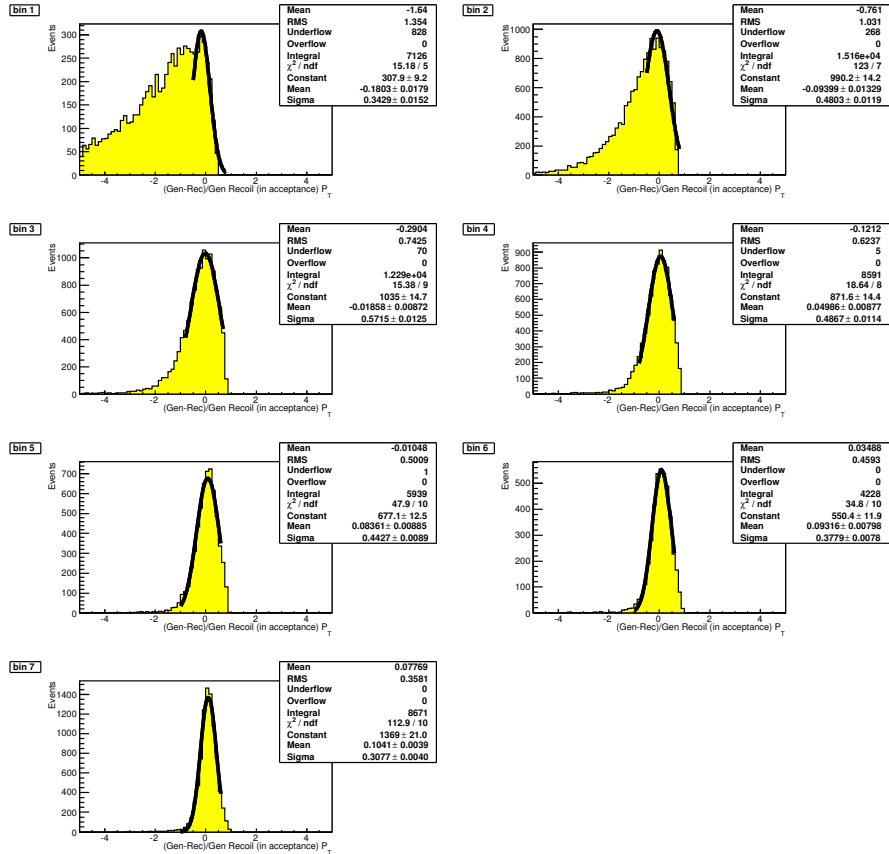


Figure 10: Absolute resolution in each of the P_T^W -bins used for the asymmetry measurement.

3.4 Background estimation

16 The background sources considered in this analysis are: $Z^0 \rightarrow e^+e^-$; $W^\pm \rightarrow \tau\nu \rightarrow e^+e^-\nu$; QCD
17 events decaying into leptons, where one of the final leptons is not detected. The first two sources

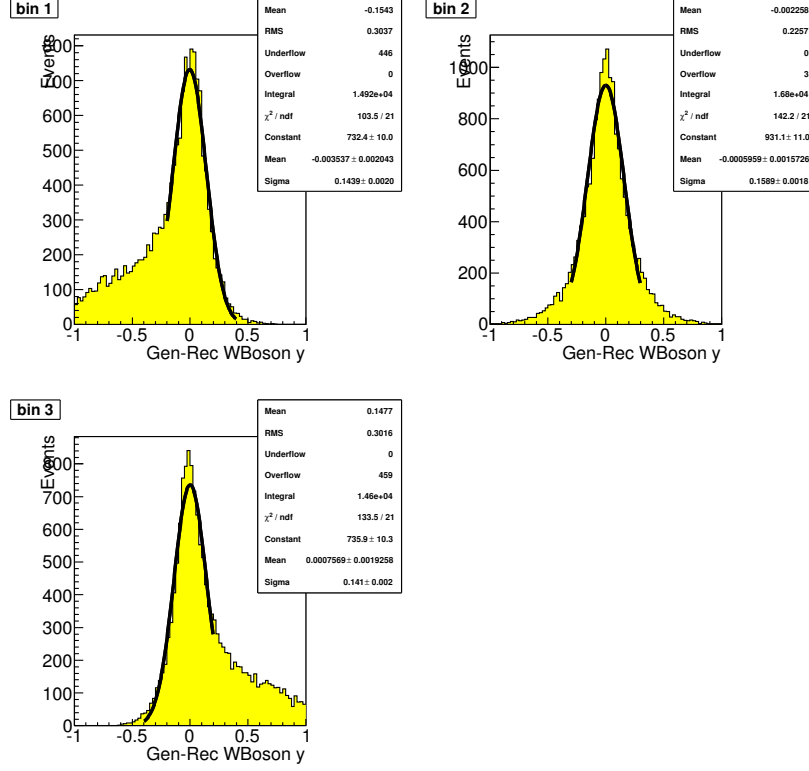


Figure 11: Absolute resolution in each of the three y^W -bins used for the asymmetry measurement.

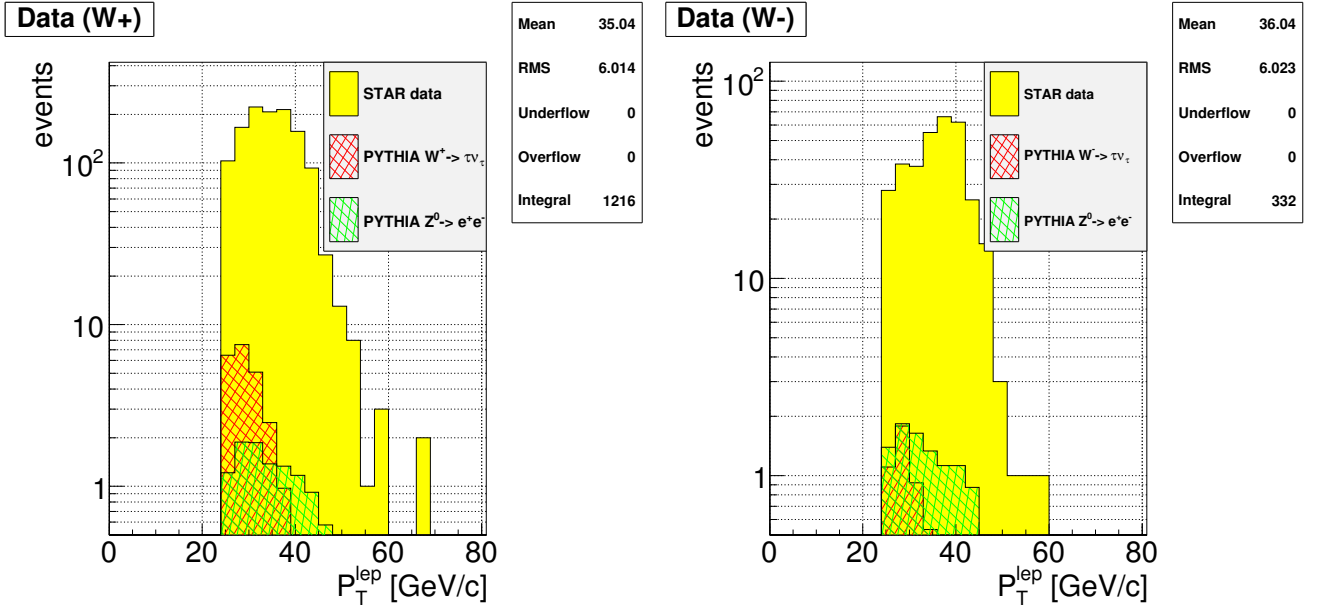


Figure 12: Estimated contribution from the $Z^0 \rightarrow e^+e^-$ and $W^\pm \rightarrow \tau\nu \rightarrow e^+e^-\nu$ backgrounds is shown for the W^+ (left) and the W^- (right) data samples respectively.

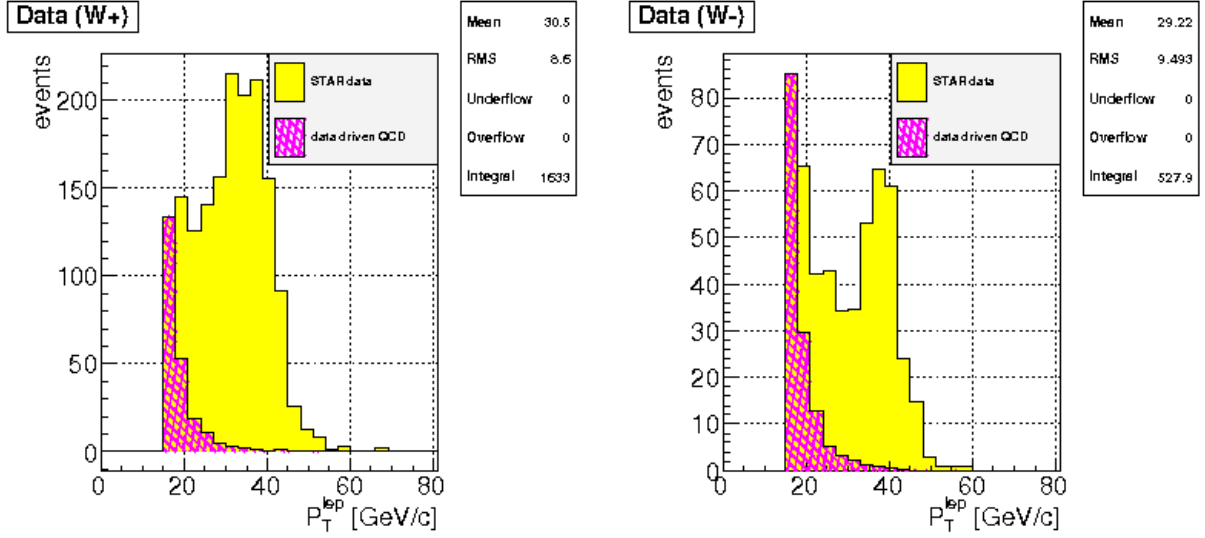


Figure 13: Estimated contribution from the QCD background is shown for the W^+ (left) and the W^- (right) data samples respectively. The data-drive QCD sample has been normalized to the lowest lepton- P_T bin.

1 have been evaluated using MC samples simulated with PYTHIA 6.4 using the “Perugia 0 tune”
2 and setting $k_T = 2$ and $CKIN(3) = 10$. The MC samples pass through the GEANT 3 simulation
3 of the STAR detector using the SL11d libraries and are embedded to the run11 p+p transverse
4 zero-bias events. To estimate the contribution from the background, the MC samples have been
5 normalized to the W^+ and the W^- data samples according to the collected luminosity as shown
6 in Fig. 12. The estimated background-over-signal values for $W^\pm \rightarrow \tau\nu$ and $Z^0 \rightarrow e^+e^-$ are shown
7 in the first columns of Table 1.

Process	$W^\pm \rightarrow \tau^\pm \nu_\tau$	$Z^0 \rightarrow e^+e^-$	QCD
B/S	1.88% (W^+); 1.39% (W^-)	0.88% (W^+); 2.94% (W^-)	1.59% (W^+); 3.40% (W^-)

Table 1: Background over signal in the W^+ and W^- samples respectively.

8 The case of background coming from QCD events is more peculiar since we cannot trust the
9 luminosity given by the MC generator. In estimating the background from this source, we followed
10 a “data-driven” technique already used at STAR for the W decay analysis with longitudinal beam
11 polarization [4, 5]. The procedure is the following:

- 12 1. a QCD dominated data sample was selected reversing the P_T -balance cut (P_T -balance <
13 15 GeV);
- 14 2. the lepton- P_T requirement in our W boson selection (see Sec. 3) was lowered to lepton-
15 $P_T > 15$ GeV;
- 16 3. the QCD data sample was normalized to the first lepton- P_T bin [15-19 GeV] as shown in
17 Fig. 13, under the assumption that this bin is dominated by QCD events with only a negligible
18 contribution from weak boson production events;

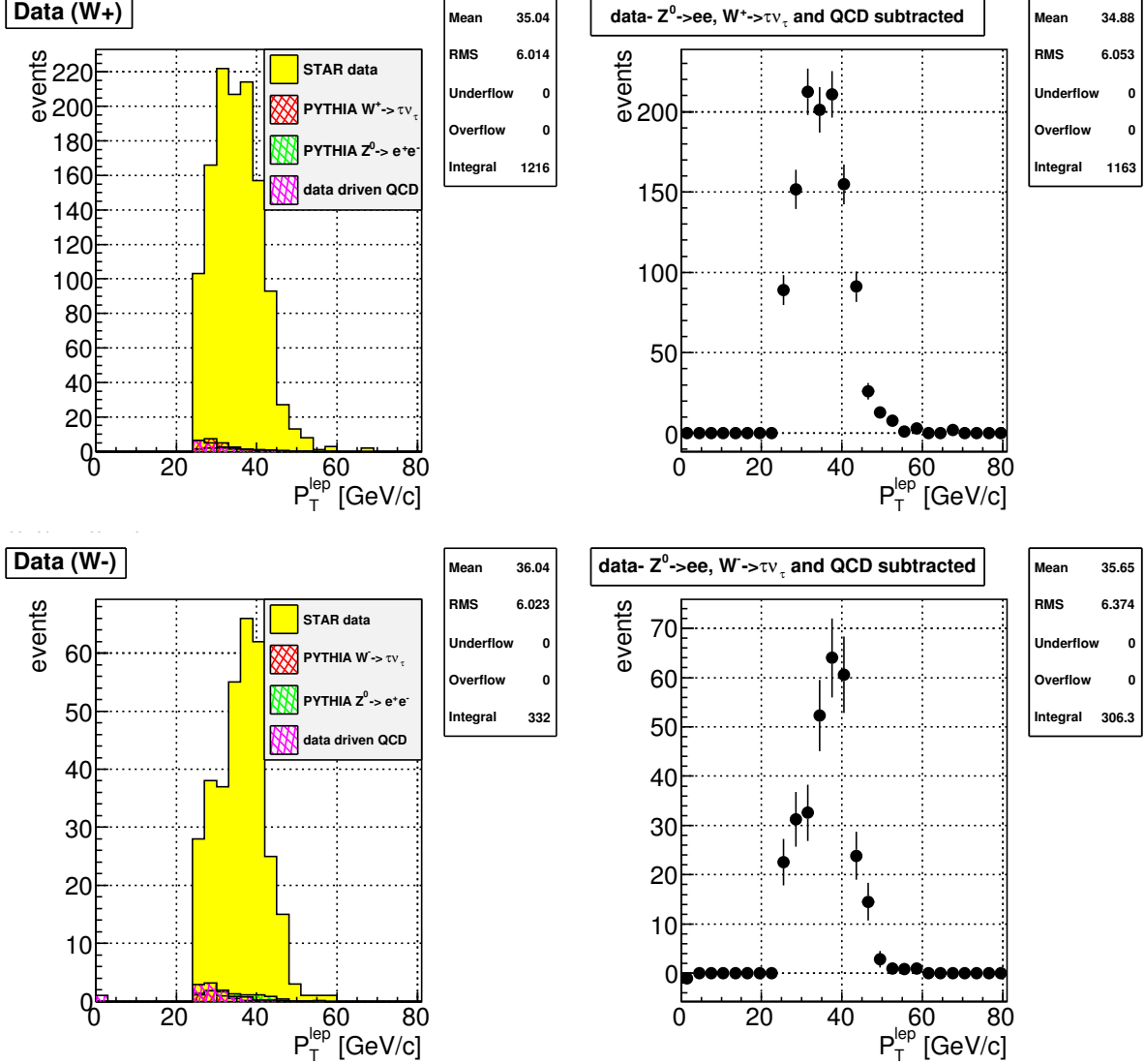


Figure 14: For the W^+ (upper row) and the W^- (lower row) data samples, figure shows the estimated contribution from the $Z^0 \rightarrow e^+e^-$, $W^\pm \rightarrow \tau\nu \rightarrow e^+e^-\nu$ and QCD backgrounds (left column), and the leptonic P_T peak after the background sources are statistically subtracted from the data sample (right column).

4. the normalized QCD sample was then compared with out signal sample after the lepton- P_T cut has been put back to its original value (lepton- $P_T > 25$ GeV), as shown if Fig. 14(*left column*).

The estimated fraction of QCD background over signal is shown in Table 1(*last column*) for the W^+ and W^- data sample separately.

From Tab. 1 one can see that background sources are under control in the present analysis, the level of background over signal contained within a few percent. Figure 14(*right column*) shows how the leptonic P_T peak looks like after the background sources are statistically subtracted from the data sample.

3.5 Systematic uncertainties

The expected systematic uncertainties due to the reconstruction procedure of the boson kinematics have been evaluated via a Monte Carlo challenge. Since PYTHIA does not have polarization implemented, we used tables (rapidity and P_T bins of W boson) of theoretical predictions for A_N with evolution included, confidentially given to us by Z-B Kang and generated from [15]. the procedure is as follows

- PYTHIA is used to generate samples for W^- production (for which A_N is predicted to be always positive);
- each prediction for A_N taken from the tables has been assigned to the PYTHIA generated values of W - y and W - P_T ;
- after the Monte Carlo events are fully reconstructed we look at the distributions of A_N in the bins of y and P_T we use for the asymmetry measurement of Sec. 5;
- the mean position of the peak in the A_N distributions at the generated and reconstructed level, in the same bins of y (Fig. 15) and P_T (Fig. 16), is compared. In the case of the distributions in bins of rapidity, a gaussian functional form has been fit to better estimate the position of the peak, as shown in Fig. 15.
- We evaluate the relative systematic uncertainty in the corresponding bin as

$$Sys(i - bin) = \frac{|mean_{i-bin}^{GEN} - mean_{i-bin}^{REC}|}{mean_{i-bin}^{GEN}}. \quad (8)$$

An additional source of common systematic normalization uncertainty on the single-spin asymmetries due to the uncertainty in the measured beam polarization has been estimated to be 3.4% [11].

4 Average polarization

Polarization of proton beams is measured at at RHIC using H-jet and P-Carbon polarimeters and the tables of results per fill (P_{Fill}) are available on-line [12]. Tables of the luminosity collected in the run 11 at STAR per each run by the W triggers are also available on-line [13] and the

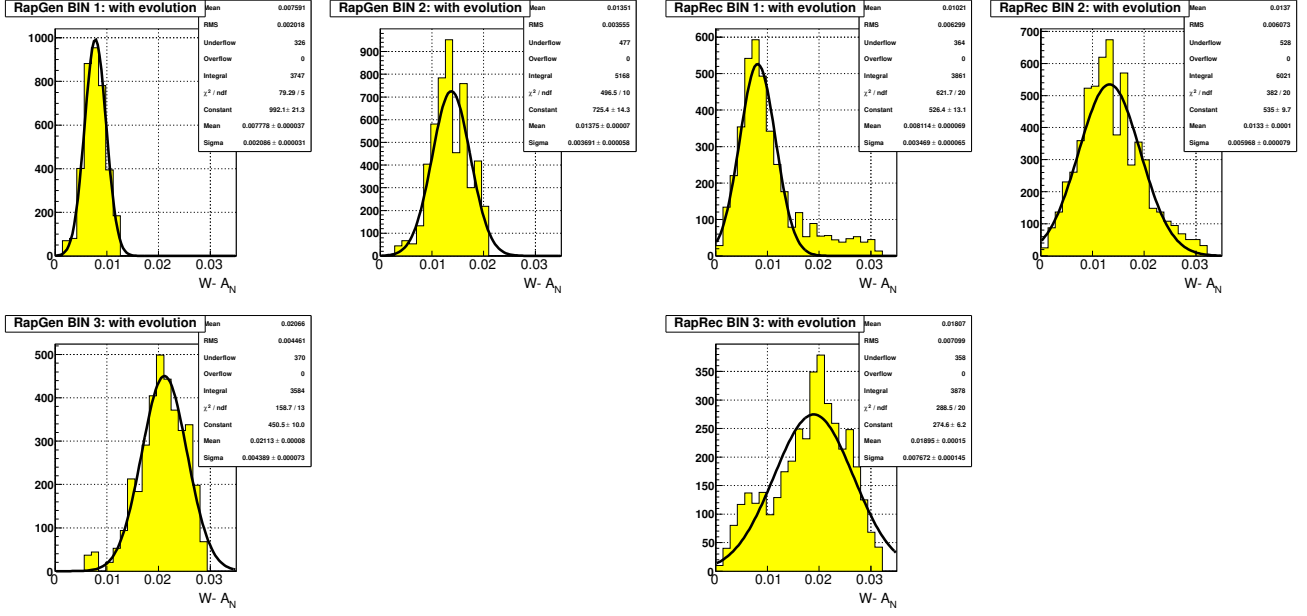


Figure 15: Distribution of A_N prediction values at the generated (*left*) and reconstructed (*right*) level for the three W-rapidity bins used in our asymmetry measurement of Sec. 5.

- 1 luminosity per fill (L_{Fill}) can be simply calculated summing up the luminosity of each run in the
- 2 fill.
- 3 Thus, the run 2011 average polarization for each beam can be calculated as follows

$$\langle P \rangle = \frac{\sum_{Fill} (L_{Fill} \cdot P_{Fill})}{\sum_{Fill} P_{Fill}} \quad (9)$$

- 4 The results are: $\langle P \rangle = 52.86\%$ for the BLUE beam and $\langle P \rangle = 52.26\%$ for the YELLOW
- 5 beam. The average value between the two beams, $\langle P \rangle = 52.56\%$, can be used for calculating the
- 6 asymmetry, as explained in Sec 5.

7 5 Asymmetry measurement

- 8 In measuring A_N we assume that the beam polarization vector does not significantly deviate from
- 9 the vertical direction given by the normal unit vector \vec{n} along the vertical y axis, $P \equiv \vec{P} \cdot \vec{n}$. We
- 10 also assume the same magnitude of the polarization vector for spin-up and spin-down bunches, *i.e.*
- 11 $P = P_{\uparrow} = P_{\downarrow}$. The single spin asymmetry A_N is expressed as:

$$A_N = \frac{\sigma_{\uparrow} - \sigma_{\downarrow}}{\sigma_{\uparrow} + \sigma_{\downarrow}}. \quad (10)$$

- 12 We bin our data sample in three observable variables, $\{y, \phi, P_T\}$, of the produced boson. Thus,
- 13 we calculated A_N using the “left-right” method [14], which helps to cancel out unwanted effects
- 14 due to geometry and luminosity.

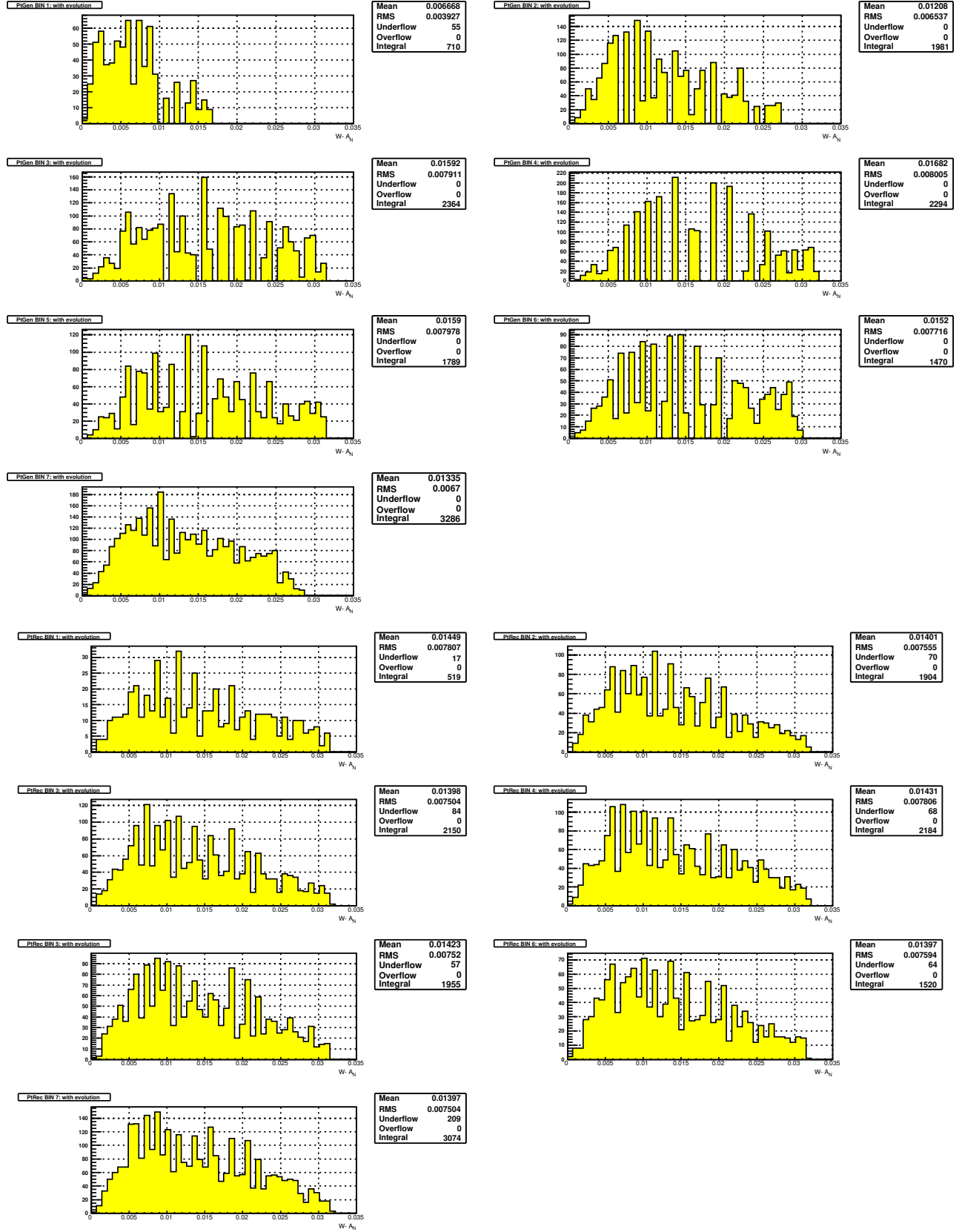


Figure 16: Distribution of A_N prediction values at the generated (*upper*) and reconstructed (*lower*) level for the seven W - P_T bins used in our asymmetry measurement of Sec. 5.

$$A_N \sin(\phi) = \frac{1}{\langle P \rangle} \frac{\sqrt{N_{\uparrow}(\phi_i)N_{\downarrow}(\phi_i + \pi)} - \sqrt{N_{\uparrow}(\phi_i + \pi)N_{\downarrow}(\phi_i)}}{\sqrt{N_{\uparrow}(\phi_i)N_{\downarrow}(\phi_i + \pi)} + \sqrt{N_{\uparrow}(\phi_i + \pi)N_{\downarrow}(\phi_i)}}, \quad (11)$$

where N is the number of recorded events in the i -th bin with a certain spin ($\uparrow\downarrow$) configuration in the “left” (ϕ_i) or in the “right” ($\phi_i + \pi$) side of the detector and $\langle P \rangle = 52.56\%$ is the average RHIC beam polarization for 2011 transverse p+p run as calculated in Sec. 4. For the asymmetry measurement the polarization of one of the beams is ignored by combining the yields with opposite spins, *e.g.*

$$N_{\uparrow} \equiv N_{\uparrow 0} = N_{\uparrow\uparrow} + R_{\frac{0\uparrow}{0\downarrow}} N_{\uparrow\downarrow}, \quad (12)$$

$$N_{\downarrow} \equiv N_{\downarrow 0} = N_{\downarrow\uparrow} + R_{\frac{0\uparrow}{0\downarrow}} N_{\downarrow\downarrow}, \quad (13)$$

where re-weighting factor $R_{\frac{0\uparrow}{0\downarrow}}$ addresses a possible relative difference in the spin-up and spin-down intensities of the other beam. Studies have shown that $R_{\frac{0\uparrow}{0\downarrow}} \approx 1$ with good precision.

The STAR preliminary results for the A_N measurement of the W^+ and W^- boson production are shown separately in Fig. 17 as a function of y^W and P_T^W . The systematic uncertainties, evaluated according to the procedure described in Sec. 3.5, are added in quadrature. The 3.4% normalization uncertainty due to the uncertainty in the beam polarization measurement is not shown in the plots.

6 The Z^0 selection and asymmetry measurement

The $Z^0 \rightarrow e^+e^-$ process has many advantages: it is experimentally very clean and the boson kinematics are easy to reconstruct since there is no neutrino in the final decay (thus it carries only the overall systematics coming from the polarization measurement), it is background free, the decay electrons peak within the STAR detector acceptance and the asymmetry is expected to be the same size as the W^\pm one. The only big disadvantage is the much lower cross section which makes the measurement very statistics hungry.

A data sample characterized by the Z^0 signature has been selected

- Two high- P_T electrons
 - lepton- $P_T > 25$ GeV;
 - $\text{Track-}|\eta| < 1$;
 - track coming from the maximum ranked vertex;
- the two electrons must have opposite charge;
- $|Z_{\text{vertex}}| < 100$ cm; vertex rank > 0 ;
- invariant mass within $\pm 20\%$ from the nominal Z^0 boson mass.

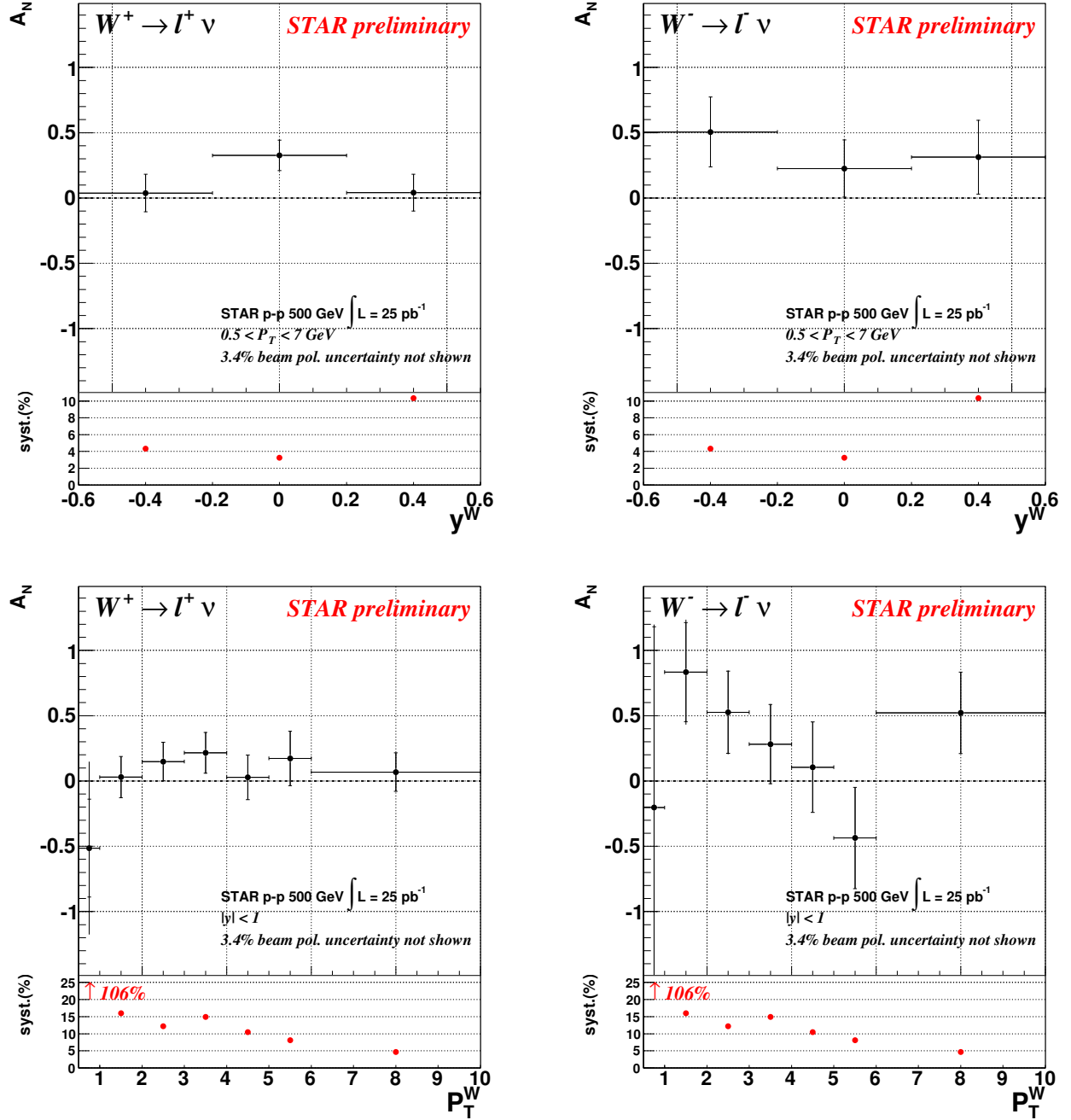


Figure 17: Transverse single spin asymmetry amplitude for W^\pm boson production, the 3.4% overall systematic uncertainty due to beam polarization is not included.

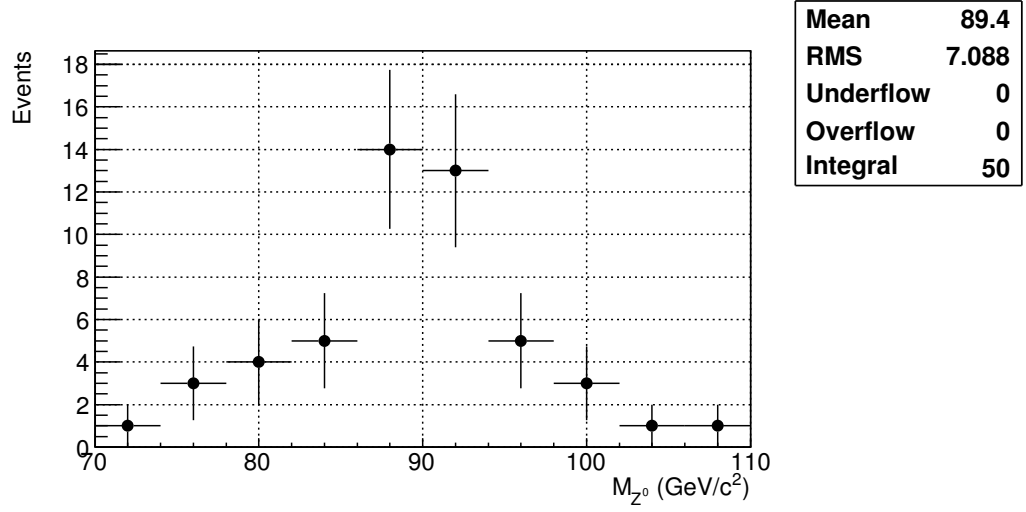


Figure 18: Invariant mass of the produced Z^0 boson.

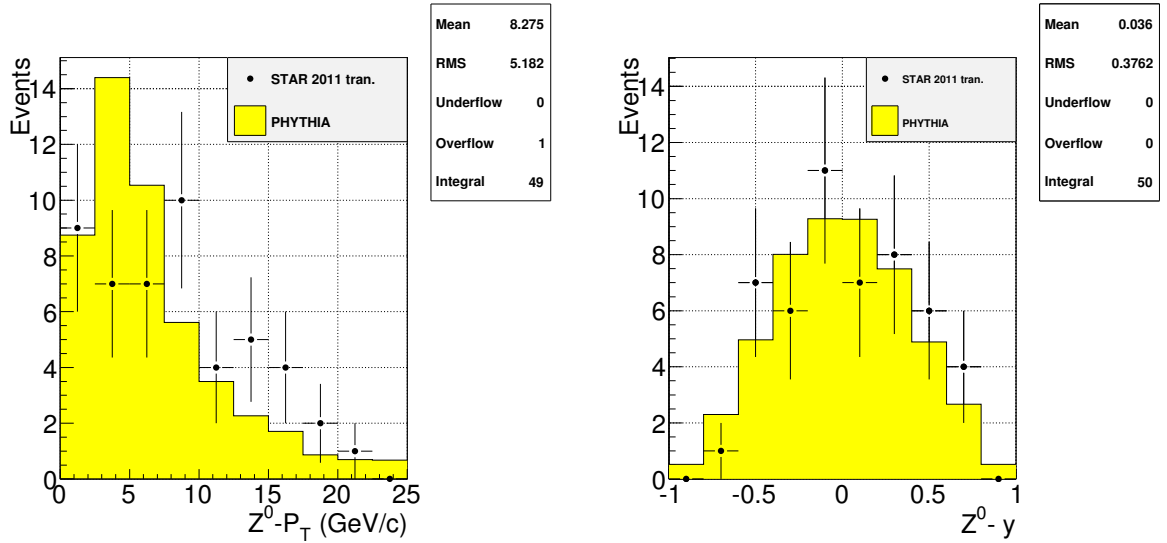


Figure 19: Data/MC agreement for the reconstructed P_T (*left*) and rapidity (*right*) of the produced Z^0 boson.

After the whole selection, only 50 events survive. The Z^0 boson invariant mass, reconstructed using this small event sample, is shown in Fig. 18. The Z^0 boson kinematics have been reconstructed from the two leptons decay, Fig. 19 shows the data/MC agreement for the reconstructed Z^0 transverse momentum and rapidity.

Due to the very small statistics we decided to measure the transverse asymmetry in a single bin for $0 < P_T < 20$ GeV and $|y^{Z^0}| < 1.5$. The STAR preliminary result for the A_N measurement of the Z^0 boson production in a single y^Z , P_T^Z bin is shown in Fig. 20.

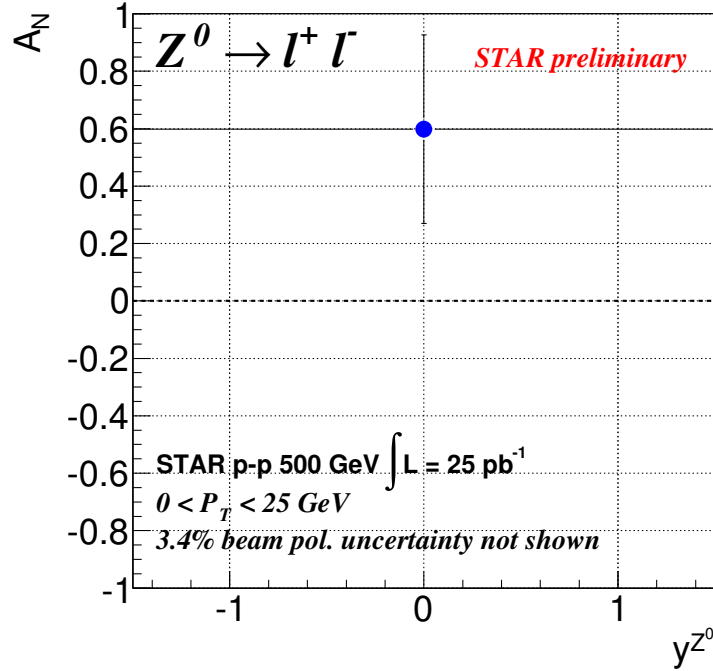


Figure 20: Transverse single spin asymmetry amplitude for Z^0 boson production, the 3.4% overall systematic uncertainty due to beam polarization is not included.

7 Conclusions and Outlook

This preliminary study is a proof-of-principle which shows that STAR is able to measure the transverse single spin asymmetries A_N for fully reconstructed W^\pm , Z^0 bosons based on a pilot run of transverse polarized p+p collisions at $\sqrt{s} = 500$ GeV with a recorded integrated luminosity of 25 pb^{-1} . The preliminary results from Fig. 17 can be compared with the most up-to-date theoretical A_N predictions for W^\pm , Z^0 boson production including TMD-evolution from reference [15], shown in Fig. 21, where the error bands have been updated accounting for the current almost complete uncertainty on sea-quark functions in the fits [16]. Measuring the production of W^\pm bosons at $\sqrt{s} = 500$ GeV can lead to the first experimental test of the sign change of the Sivers function. Furthermore, it provides an ideal tool to study the spin-flavor structure of sea quarks inside the proton. The left-handed W boson only couples to (anti)quarks of a certain helicity, giving rise to large parity-violating single spin asymmetries. In addition, the coupling of the W to the weak charge correlates directly to quark flavor. Ignoring quark mixing, W^\pm bosons are produced

through $u + \bar{d}(d + \bar{u})$ interactions. A measurement of the transverse single spin asymmetry will provide the worldwide first constraint on the sea quark Sivers function in an x-range, where the measured asymmetry in the \bar{u} and \bar{d} unpolarized sea quark distribution functions, as measured by E866 [17], can only be explained by strong non-pQCD contributions. Figure 22 shows the projected uncertainties for transverse single spin asymmetries of W^\pm , Z^0 bosons as functions of rapidity and P_T for a delivered integrated luminosity of 900 pb^{-1} compared to 400 pb^{-1} , at an average beam polarization of $\sim 55\%$. RHIC is capable of delivering 900 pb^{-1} in 14 weeks running using a dynamic β^* squeeze [18] through the fill. The dynamic β^* squeeze provides a factor 2 increase of the luminosity in a fill as the luminosity profile through the fill is kept flat.

STAR is the only experiment capable of measuring A_N for direct photons, for W^\pm and Z^0 bosons, and possibly for DY. It can provide a world-wide unique opportunity to simultaneously test TMD evolution, access the Sivers function for sea quarks, and test the predicted sign-change for the Sivers function.

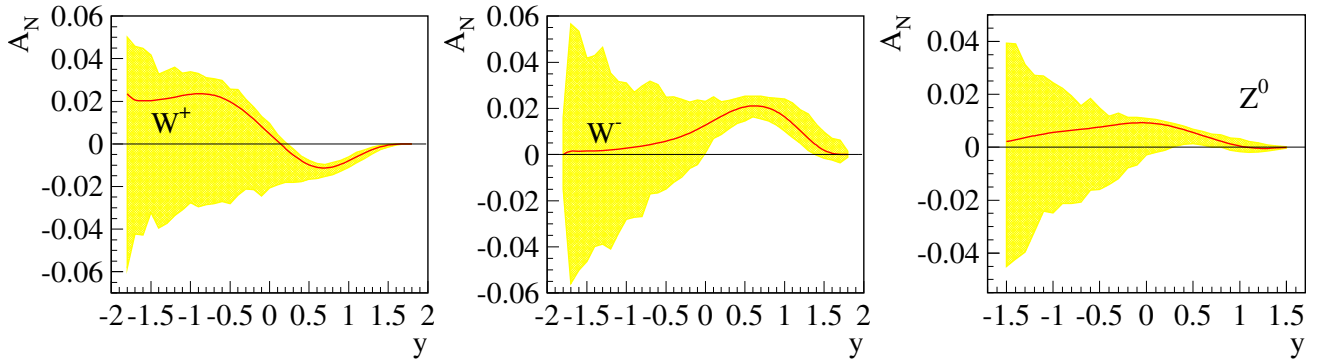


Figure 21: Theoretical prediction of A_N for W^\pm and Z^0 boson production in p+p collisions at $\sqrt{s} = 500 \text{ GeV}$ including TMD-evolution [15].

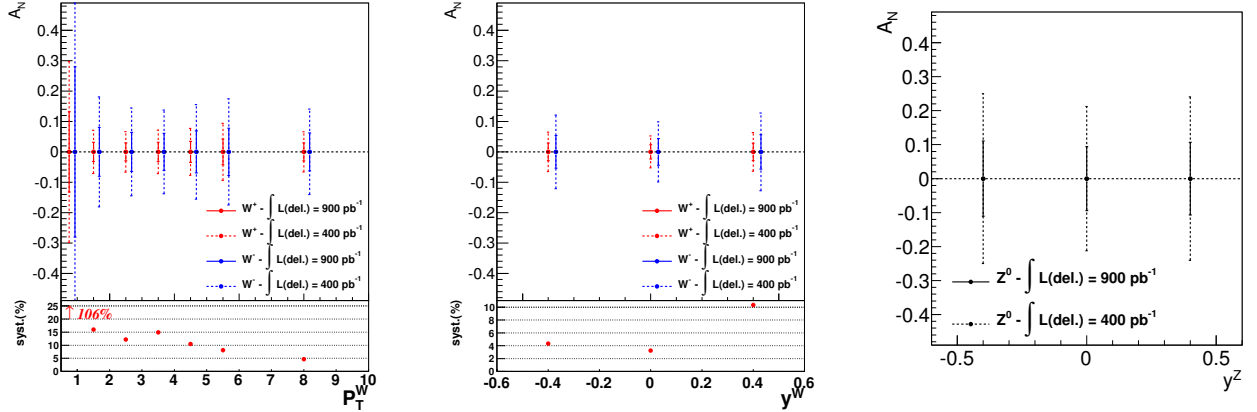


Figure 22: Projections of statistical uncertainties of an A_N measurement for W^\pm and Z^0 boson production at STAR assuming a delivered luminosity of 900 pb^{-1} , the 400 pb^{-1} case is also shown for comparison.

1 A Extraction of the analyzing power, A_N

2 The Transverse Single Spin Asymmetry has been calculated as in Eq. 5 and the A_N amplitude has
3 been extracted binning our data in four ϕ ($\phi + \pi$) bins and performing a $\sin(\phi)$ modulation fit per
4 each bin in P_T^W and y^W . The $\sin(\phi)$ fits have been performed assuming a $\pi/2$ phase according
5 to STAR coordinates. The asymmetries from geometry and luminosity effects have been also
6 separately extracted.

7 A collection of the latest results for the asymmetry including blue and yellow beam asym-
8 metries extracted separately, asymmetries from the geometry and luminosity effects, asymmetries
9 calculated from the decay lepton and all the $\sin(\phi)$ modulations fits can be downloaded in the
10 STAR drupal page:

11 https://drupal.star.bnl.gov/STAR/system/files/asymmetry_results.zip

12 Results can also be easily accessed via a web interface at the following webpage:

13 <http://www.star.bnl.gov/~fazio/vbasym/webview/>

14 B Reproduction of results

15 The code used for the present analysis is in the CVS repositories at the link

16 <http://www.star.bnl.gov/cgi-bin/protected/cvsweb.cgi/offline/users/fazio/vbasym/>

17 B.1 How to check out and build the analysis code

18 To check the code out, from the location where the package will be installed on your machine issue
19 the following command:

```
20 cvs co -d vbasym offline/users/fazio/vbasym/
```

23 Before you can build and run the program the following environment variables must be set:

```
24 VBASYM_DIR
```

27 this variable contains the path to the project directory

```
28 VBASYM_RESULTS_DIR
```

31 this variable contains the path to the output directory where the results will be put.

32 The following environment variables are assumed to be set in the standard STAR session:

```
33 STAR_VERSION  
34 STAR_HOST_SYS  
35 ROOTSYS
```

38 Example scripts setting up these variables can be found in the “scripts/” directory:

```
39 scripts/setup.sh  
40 scripts/setup.csh
```

43 To build the library run a slightly modified “cons” command in the terminal

```
44 cd $VBASYM_DIR  
45 cons CXXFLAGS="-m32 -fPIC -pipe -Wall -Woverloaded-virtual -Wno-  
46 long-long" \
```

```
EXTRA_CXXFLAGS="-I${OPTSTAR}/include -Icontrib/root-helper" \
CPPPATH="#:#StRoot:#.sl64-gcc447/include:${ROOTSYS}/include
:./ contrib/root-helper"
```

The binaries are compiled by issuing the following command:

```
mkdir build
cd build
cmake28 .. -DBOOST_ROOT=${OPTSTAR}
make
```

B.2 How to split the Monte Carlo file lists

Embedded Monte-Carlo (MC) files relevant for this analysis were produced using PYTHIA and are stored on the STAR data disks. The file lists are contained in “\$VBASYM_DIR/runlists” with the following format used for their names: “<run period>_mc<process type>”. For example, “run11_mc_Wp2enu” is a file list for the $W^+ \rightarrow e\nu$ MC embedded with Run 11 zero bias events.

The list may contain a large number of files. It is convenient, when submitting a job to *condor*, to split very long lists into several sublists or “runs”. To split it do:

```
cd $VBASYM_DIR/runlists/
split -d -l <# of lines in each sublist> <list name> <list name>_
```

For example, executing the command

```
split -d -l 5 run11_mc_Z02ee run11_mc_Z02ee_
```

will split the content of the list “run11_mc_Z02ee” in many sublist each containing 5 lines of the original list and numbered in numerical order starting with 00. In your directory you should see files named:

```
run11_mc_Z02ee_00
run11_mc_Z02ee_01
run11_mc_Z02ee_02
...
```

Now all you have to do is to create a text file containing the names of this sublists you just created. For example create the file named

```
run11_mc_Z02ee_
```

and copy in it the list

```
run11_mc_Z02ee_00
run11_mc_Z02ee_01
run11_mc_Z02ee_02
...
```

Now all what is needed it to submit to condor the file “run11_mc_Z02ee_”. The next section explains how to submit to condor.

2 B.3 How to produce the analysis ROOT trees

3 To produce the jet root trees do:

```
4 cd $VBASYM.DIR/scripts
5 submit_jobs.sh run12_pp_j3 -z -r12 --jets
6
```

8 Then to produce the analysis root trees do:

```
9 submit_jobs.sh run12_pp_j3 -z -r12
10
11
```

12 Other examples:

```
13 submit_jobs.sh run11_pp_transverse --jets
14 submit_jobs.sh run11_pp_transverse
15 submit_jobs.sh run11_mc_Wp2enu_ -m --jets
16
17
```

18 B.4 How to check condor jobs output

19 One can check the output files returned by condor by verifying the “tralala” marker in the log
20 files. There should be just one entry per log file:

```
21 grep tralala /path/to/log/* > /tmp/check_jobs_tralala &
22 diff --suppress-common-lines -y $VBASYM.DIR/runlists/
23 run11_pp_transverse /tmp/check_jobs_tralala
24
25
```

26 B.5 How to produce histograms from ROOT trees

27 Various sets of histograms can be produced from the ROOT trees generated with ‘stana’. This
28 stage of the analysis is done with the help of ‘vbana’ executable. One can run

```
29 vbana -f run11_pp_transverse
30
31
```

32 and on the MC samples:

```
33 vbana -f run11_mc_Wp2enu_
34
35
```

36 For help with other options run “vbana -h”.

37 C Run list

38 The list of STAR runs used in this analysis is the following

```
39
40 12038078 12038079 12038080 12038081 12038082 12038086 12038087 12038088 12038089 12038092
41 12038106 12038108 12038115 12042026 12042027 12042028 12042029 12042030 12042033 12042034
42 12042035 12042036 12043044 12043045 12043046 12043047 12043048 12043049 12043051 12043052
43 12043053 12043055 12043060 12043065 12043066 12043067 12043068 12043069 12043077 12043078
44 12043079 12043081 12044023 12044024 12044025 12044026 12044029 12044030 12044031 12044038
45 12044039 12044040 12044041 12044042 12044043 12044050 12044051 12044052 12044053 12044054
1 12044055 12044079 12044080 12044088 12044091 12044092 12044093 12044094 12044096 12044097
```

2 12044098 12044099 12044100 12044101 12044102 12044103 12045001 12045002 12045004 12045005
 3 12045006 12045011 12045013 12045016 12046035 12046036 12046037 12046038 12046039 12046040
 4 12046041 12046042 12046043 12046046 12046068 12046069 12046070 12046075 12046095 12046097
 5 12046098 12046099 12046100 12046101 12046102 12046103 12046104 12046105 12046106 12046107
 6 12047009 12047011 12047016 12047017 12047018 12047019 12047020 12047021 12049037 12049038
 7 12049042 12049043 12049044 12049067 12049069 12049070 12049071 12050022 12050023 12050024
 8 12050034 12050035 12050037 12050038 12050039 12050040 12050041 12050042 12050044 12050045
 9 12050046 12050047 12050048 12051006 12051007 12051008 12051009 12051010 12051011 12051012
 10 12051013 12051014 12051020 12051021 12051022 12051023 12051024 12051025 12051026 12051027
 11 12051028 12051029 12051030 12051031 12051032 12051033 12051034 12051035 12051036 12051037
 12 12051038 12051052 12051053 12051054 12051055 12051056 12051057 12051059 12051062 12051063
 13 12051064 12051065 12052011 12052012 12052013 12052014 12052018 12052019 12052020 12052021
 14 12052022 12052023 12052024 12052026 12052027 12052028 12052029 12052030 12052031 12052032
 15 12052033 12052034 12052047 12052048 12052049 12052050 12052051 12052054 12053005 12053006
 16 12053007 12053008 12053009 12053010 12053011 12053013 12053031 12053036 12053039 12053040
 17 12053041 12053042 12053043 12053044 12053048 12053049 12053050 12053051 12053052 12053054
 18 12053056 12053057 12053058 12053070 12054013 12054014 12054015 12054016 12054017 12054018
 19 12054019 12054020 12054021 12054022 12054024 12054025 12054026 12054027 12054028 12054029
 20 12054030 12055031 12055034 12055035 12056007 12056008 12056009 12056010 12056011 12056012
 21 12056013 12056014 12056015 12056016 12056017 12056018 12056019 12056020 12057008 12057009
 22 12057010 12057011 12057012 12057013 12057014 12057016 12057017 12057018 12057019 12057020
 23 12057022 12057050 12057051 12057052 12057053 12057054 12057055 12057057 12057058 12057059
 24 12057060 12058001 12058003 12058004 12058005 12058011 12058012 12058013 12058014 12058015
 25 12058016 12058017 12058018 12058019 12058021 12058022 12058024 12058040 12058048 12058049
 26 12058050 12058052 12058054 12058055 12058057 12058058 12059006 12059007 12059008 12059009
 27 12059010 12059011 12059012 12059013 12059016 12059017 12059018 12059019 12059020 12059021
 28 12059024 12059027 12059028 12059029 12059030 12059031 12059035 12059036 12059037 12059038
 29 12059039 12059070 12059071 12059077 12059078 12059079 12059080 12059082 12059083 12059084
 30 12060001 12060004 12060005 12060006 12060007 12060009 12060010 12060011 12060030 12060033
 31 12060034 12060035 12060036 12060037 12060038 12060039 12060040 12060041 12060042 12060043
 32 12060044 12060045 12060046 12060047 12060048 12060049 12060051 12060056 12060058 12060138
 33 12060143 12060144 12060145 12060146 12061006 12061008 12061010 12061011 12061013 12061014
 34 12061015 12061016 12061018 12062011 12062012 12062013 12062014 12062015 12062016 12062017
 35 12062018 12062019 12062021 12062022 12064003 12064005 12064007 12064008 12064010 12064011
 36 12064012 12064013 12064014 12064015 12064016 12064026 12064027 12064028 12064029 12064033
 37 12064034 12064035 12064036 12064040 12064042 12064043 12064044 12064045 12064058 12064059
 38 12064060 12064061 12064062 12064063 12064064 12064065 12064066 12064067 12064068 12064069
 39 12064070 12064071 12064084 12064085 12064086 12064087 12064088 12064090 12065001 12065004
 40 12065006 12065007 12065009 12065011 12065016 12065018 12075019 12075021 12075022 12075024
 41 12075025 12075027 12075028 12075029 12075030 12075031 12075032 12075033 12075034 12075039
 42 12075040 12075041 12075042 12075043 12076002 12076007 12076008 12076009 12076028 12076029
 43 12076031 12076034 12079005 12079026 12079027 12079028 12079030 12079031 12079038 12079039
 44 12079040 12079041 12079042 12079043 12079045 12079046 12079047 12079049 12079050 12080001
 45 12080004 12080010 12080011 12080012 12080017 12080018 12080020 12080052 12080053 12080054
 46 12080055 12080058 12080059 12080062 12080064 12080066 12080067 12080068 12080069 12080070
 47 12081009 12081011 12081012 12081013 12081014 12081015 12081016 12081020 12081021 12081022
 1 12081023 12081024 12081025 12081027 12081050 12081052 12081053 12081055 12081056 12081057

2 12081069 12081070 12082001 12082002 12082003 12082004 12082005 12082007 12082022 12082023
 3 12082024 12083011 12083012 12083013 12083014 12083016 12083017 12083018 12083019 12083020
 4 12083021 12083022 12083023 12083024 12083045 12083046 12083047 12083050 12083051 12083052
 5 12083053 12083054 12083055 12083056 12083057 12083058 12083059 12083060 12083061 12084004
 6 12084009 12084010 12084011 12084012 12084013 12084014 12084015 12084016 12084017 12084018
 7 12084019 12084020 12084021 12085023 12085024 12085025 12085026 12085027 12085028 12085029
 8 12085030 12085031 12086001 12086002 12086004 12086005 12086006 12086007 12086017 12086019
 9 12086020 12086033 12086034 12086035 12086037 12086038 12086039 12086040 12086041 12086042
 10 12086046 12086047 12087002 12087003 12087004 12087005 12087012 12087023 12087025 12087026
 11 12087027 12087032 12087033 12087034 12087036 12087038 12087045 12087053 12087054 12087080
 12 12087084 12087085 12087095 12087096 12087097 12087098 12087099 12087100 12087101 12087102
 13 12088022 12088026 12088028 12088030 12088031 12088032 12088033 12088034 12088035 12088049
 14 12088050 12088075 12088076 12088077 12088078 12088079 12088080 12088081 12088086 12088087
 15 12088088 12089006 12089008 12089009 12089010 12089011 12089085 12089086 12089087 12089088
 16 12090002 12090003 12090006 12090007 12090009 12090010 12090011 12090017 12090019 12090020
 17 12090021 12090022 12090042 12090043 12090045 12090046 12090047 12090048 12090049 12090050
 18 12090051 12090052 12090053 12090054 12090055 12090060 12091004 12091005 12091006 12091007
 19 12091009 12091010 12091011 12091012 12091013 12091014 12091016 12091017 12091018 12091019
 20 12091021 12091022 12091023 12091041 12091042 12091043 12091044 12091045 12091046 12091047
 21 12091048 12091049 12091051 12091052 12091053 12091054 12092001 12092002 12092003 12092004
 22 12092005 12092020 12092021 12092037 12092038 12092047 12093001 12093002 12093003 12093004
 23 12093005 12093006 12093007 12093008 12093009 12093010 12093011 12093012 12093014 12093023
 24 12093024 12093025 12093030 12093031 12093032 12093033 12093034 12093036 12093037 12093039
 25 12093040 12093041 12093042 12093044 12093049 12093050 12093051 12094009 12094010 12094011
 26 12094012 12094013 12094014 12094015 12094016 12094017 12094018 12094019 12094020 12094021
 27 12094022 12094024 12094025 12094026 12094060 12094061 12094062 12094063 12094064 12094065
 28 12095005 12095006 12095008 12095010 12095011 12095012 12095013 12095021 12095022 12095023
 29 12095038 12095039 12095041 12095042 12095043 12095044 12095045 12095046 12095050 12095052
 30 12095054 12095055 12095056 12095057 12095058 12095059 12095060 12095061 12095063 12096005
 31 12096006 12096014 12096015 12096016 12096017 12096018 12096019 12096020 12096021 12096023
 32 12096024 12096025 12096026 12096027 12096028 12096029 12096030 12096031 12096032 12096033
 33 12096034 12096047 12096048 12096049 12096056 12096057 12096058 12096059 12096060 12096061
 34 12096062 12097002 12097003 12097004 12097007 12097008 12097009 12097010 12097011 12097012
 35 12097013 12097016 12097017 12097018 12097019 12097020 12097021 12097022 12098008 12098009
 36 12098010 12098012 12098013 12098014 12098017 12098018 12098019 12098020 12098021 12098022
 1 12098030 12098031

References

- [1] Z. -B. Kang and J. -W. Qiu, “Testing the Time-Reversal Modified Universality of the Sivers Function,” *Phys. Rev. Lett.* **103**, 172001 (2009) [arXiv:0903.3629 [hep-ph]].
- [2] M. Aggarwal et al. (STAR), Measurement of the parity-violating longitudinal single-spin asymmetry for W^\pm boson production in polarized proton-proton collisions at $\sqrt{s} = 500$ GeV, *Phys. Rev. Lett.* **106**, 062002 (2011), arXiv:1009.0326 [hep-ex].
- [3] J. Balewski, J. Seele, J. Stevens, and O. Grebenyuk, Measurement of the parity-violating longitudinal single-spin asymmetry A_L for W^+ and W^- boson production in polarized $\vec{p} + p$ collisions at $\sqrt{s} = 500$ GeV in Run 9 (STAR Note # 516), (2010).
- [4] L. Adamczyk et al. (STAR), Measurement of longitudinal spin asymmetries for weak boson production in polarized proton-proton collisions at RHIC, *Phys. Rev. Lett.* **113** (2014) 072301, arXiv:1404.6880 [nucl-ex]
- [5] J. Balewski, J. Stevens, and J. Zhang, Measurement of the parity-violating longitudinal single-spin asymmetry for weak boson production in polarized proton-proton collisions in Run 11 + 12 at $\sqrt{s} = 510$ GeV (STAR Note # 597), (2013).
- [6] P. M. Nadolsky and C.-P. Yuan, Single-spin physics with W bosons at RHIC, *Nucl. Phys. B* **666**, 31 (2003)
- [7] G. Altarelli, R. K. Ellis, and G. Martinelli, *Z. Phys. C - Particles and Fields* **27**, 617-632 (1985)
- [8] C. Albajar et al., the UA1 Collaboration, *Z. Phys. C - Particles and Fields* **44**, 15-61 (1989)
- [9] L. Adamczyk et al. (STAR), Measurement of the $W \rightarrow e\nu$ and $Z^0/\gamma^* \rightarrow e^+e^-$ production cross sections at mid-rapidity in proton-proton collisions at $\sqrt{s} = 500$ GeV, *Phys. Rev. D* **85**, 092010 (2012), arXiv:1112.2980 [hep-ex].
- [10] J. Stevens, Measurement of the $W \rightarrow e\nu$ and $Z^0/\gamma^* \rightarrow e^+e^-$ Production Cross Sections at Mid-rapidity in Proton-Proton Collisions at $\sqrt{s} = 500$ GeV in Run 9 (STAR Note # 546), (2011).
- [11] RHIC Polarimetry Group, RHIC/CAD Accelerator Physics Note, 490 (2013).
- [12] RHIC Polarimetry Results by Fill
<http://www.phy.bnl.gov/cnipol/fills/>
- [13] STAR run 11 collected luminosity per run in the W triggers
http://www.star.bnl.gov/protected/common/common2011/trigger2011/lumi500GeV/lum_perrun_BHT3*L2BW.txt
- [14] Bültmann S et al. *Phys. Lett. B* **632** 167 (2006)
Bültmann S et al. *Phys. Lett. B* **647** 98 (2007)
Ohlsen G G and Keaton Jr P W 1973 *Nucl. Instr. Meth.* **109** 41
- [15] M. G. Echevarria, A. Idilbi, Z.-B. Kang, I. Vitev, *Phys. Rev. D* **89**, 074013 (2014)
- [16] Z.-B. Kang, private communication

- ² [17] E. A. Hawker et al. *Phys. Rev. Lett.* **80**, 3715 (1998)
- ⁵⁶⁸ [18] D. Trbojevic, J. Yichao, Y. Luo, BNL-102458-2013-CP